Equilibrium Partitioning of a Dimerizing Fluid Through a Microporous Solid: A Monte Carlo Study of the Density Distributions and Adsorption Isotherms

Youri Duda,[†,⊥] Douglas Henderson,[‡,||] Beatriz Millan-Malo,[§] and Orest Pizio*[,†]

Instituto de Química de la UNAM, Circuito Exterior, Coyoacán 04510, México D.F., Department of Chemistry and Biochemistry, Brigham Young University, Provo, Utah 84602, and Instituto de Física de la UNAM, Circuito Exterior, Coyoacán 04511, Mexico D.F.

Received: June 13, 1997; In Final Form: September 24, 1997[⊗]

We have considered a simple, hard-core-type model for an inhomogeneous system consisting of a dimerizing fluid and a microporous solid membrane with a slit shape. The system is confined to a wide slitlike pore. The bulk and porous regions are in thermodynamic equilibrium. Monte Carlo canonical simulation results are presented for the density distributions of the particles in the bulk fluid region, in layers close to the outer surfaces of the porous solid and inside the crystalline membrane. We have observed that dimers prefer to be located in the interstices of the membrane channels rather than in the membrane cavities. The pressure is obtained from the density profiles on the walls of a wide pore. We show that the adsorption isotherms and the partition coefficients are sensitive to the association energy between fluid particles. For almost all densities, the partition coefficient of the monomers is found to be higher than for those particles that belong to dimers. This reflects the shape selectivity of the membrane with respect to the fluid species during adsorption.

1. Introduction

The study of chemically associating *inhomogeneous* fluids has been initiated and has attracted much attention in the last years.[1−13] Usually, systems restricted by simple geometric constraints, such as walls and/or individual slit-like pores, have been investigated. In some cases, the crystalline symmetry of the adsorbing atoms in the pore walls have been included.[12−16] Computer simulations, density functional techniques, and an integral equation method have been used successfully as theoretical tools in this area.

In the present work, we turn out our attention to the problem of chemically associating fluids confined in a microporous medium. In contrast to our recent studies of chemical association in disordered porous systems,[17−20] we focus on the case of a microporous solid with a highly symmetric distribution of the porous space. The investigation of adsorption and chemical reactions in microporous solids is of interest from a basic point of view. Besides, it is of relevance for applications in membrane separations and heterogeneous catalysis by zeolites. From a simplified view, zeolite structure is characterized by the presence of a regular network of pores and cavities, whose diameter is commensurate with the molecular dimensions.

A simple model for the adsorption of a simple fluid in a microporous solid has been proposed and investigated recently by Dong and Bigot.[21] These authors have considered a two dimensional fluid, consisting of hard discs, which is equilibrated between a 'bulk' region in contact with a slit of membrane particles in a crystal configuration of the (10) "plane". The particles of the membrane have been assumed to form a "dilute" medium, in which the fluid particles are free to move. However, the fluid has been studied at only one density. The main focus has been put on the symmetry factors and the diameter of membrane species and the size of the pores. To obtain a detailed description of the density distributions close to the outer "planes" of the membrane, i.e., between the fluid bulk and the membrane interior, NVT Monte Carlo simulations have been performed. These simulations consider the fluid in a sufficiently large membrane-free volume and, simultaneously, in the membrane interior in order to reach a true equilibrium between the two systems. This approach has been proposed previously by Yethiraj and Hall to simulate a fluid in the bulk and in a slitlike pore.[22]

One particular objective in this work is the extension of the study of Dong and Bigot[21] for a nonassociating simple fluid to a chemically associating fluid. Moreover, we have performed additional simulations for nonassociating discs to characterize the fluid partitioning at different fluid pressures. Similar to Yethiraj and Hall,[22] we have confined a chemically associating system in a wide pore. The contact value of the density profile on a wall of a wide pore yields the pressure straightforwardly. In this manner, we have obtained the adsorption isotherms for the nonassociating and associating fluids. As discussed by Dong and Bigot,[21] the exterior region of a membrane can play an important role in some processes. They have found lateral density variations that are of similar importance as the variations in the normal direction (perpendicular to the outer solid surface).

One of the primary objectives of our study in the case of a dimerizing system is the investigation of issues related to the shape selectivity of a crystalline membrane. For different values of the equilibrium dimerization constant, we expect different partitioning of the monomer and dimer species. One more interesting aspect of this problem is the insight into the distribution of the orientations of dimer species in the membrane interior that is obtained.

In this work, similar to ref 21, we restrict our attention to two-dimensional (2D) models; we do this only to make the simulations more time efficient. However, we are confident that our conclusions will be valid for the three-dimensional counterpart of the model, at least qualitatively. Two-dimensional models have been used previously to simulate the dynamics of fluid passage through a microporous membrane, see for example; ref 23 for some more complicated models for fluid adsorption in microporous solids.[24,25] However, a thorough

[⊥] Permanent address: Institute for Condensed Matter Physics, National Academy of Sciences of the Ukraine, Lviv 11, Ukraine.
[||] John Simon Guggenheim Memorial Foundation Fellow.
[†] Instituto de Química de la UNAM.
[‡] Department of Chemistry and Biochemistry.
[§] Instituto de Física de la UNAM.
[⊗] Abstract published in *Advance ACS Abstracts,* November 15, 1997.

S1089-5647(97)01948-2 CCC: $14.00

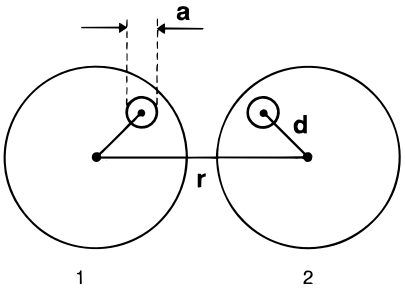

Figure 1. The geometry of the interactions between fluid particles.

study of the equilibrium partitioning of chemically associating fluids is needed before investigating their dynamic properties.

We describe first the model and simulation procedure. Next the results of simulations are presented and discussed. Finally we draw some conclusions and outline a few future objectives.

2. Model for a Dimerizing Fluid Equilibrated between Its Bulk and a Crystalline Membrane

For simplicity, we restrict ourselves to a model of a dimerizing fluid of the type: $A + A \rightleftharpoons A_2$.[26] In this model the dimerization takes place due to finite range, strong attractive interactions between the sites located inside a hard core of particles or on their surface. The interaction potential between fluid species is assumed to have the form

$$U(1, 2) = U_{\text{non}}(r_{12}) + U_{\text{as}}(\xi_{12}) \tag{1}$$

where $\xi_{12} = | \mathbf{r}_{12} + \mathbf{d}(\Omega_1) - \mathbf{d}(\Omega_2) |$, $\mathbf{d}(\Omega)$ denotes the position and orientation of the attractive interaction site embedded into the core that is defined by nonassociative term. Hereinafter, all vectors are two-dimensional, $\mathbf{r} = \mathbf{r}(x, y)$. The nonassociative term, $U_{\text{non}}(r_{12})$, is given as

$$U_{\text{non}}(r) = \begin{cases} \infty, & r < L \\ D, & L < r < \sigma_f \\ 0, & r > \sigma_f \end{cases} \tag{2}$$

Without any loss of generality, the fluid particle diameter is taken as the length unit, $\sigma_f = 1$. The associative interaction is

$$U_{\text{as}}(\xi) = \begin{cases} -\epsilon_{\text{as}}, & \xi \le a \\ 0, & \xi > a \end{cases} \tag{3}$$

where ϵ_{as} and a are the association energy and range of attraction, respectively, L is the bonding length, and D is the height of the square mound. The parameter D is irrelevant; it is a large constant to provide $\exp(-\beta D) \simeq 0$ and $\beta = 1/kT$. The parameters of the interaction are chosen to satisfy the geometric condition, $L < 2d + a < L + (2 - \sqrt{3})d$, $d = |\mathbf{d}(\Omega)|$, in order to ensure steric saturation at dimer level, i.e., there is no double bonding to a given attractive site.[26] The fluid model geometry is shown in Figure 1 for the sake of better understanding of the reader.

We choose the following set of parameters in this work: $L = 0.9$, $d = 0.45$, and $a = 0.1$. Further, we assume that the particles of the solid are hard discs with the diameter σ_s. The solid particles are confined in a slit, inside the slit they are located on a square lattice whose lattice sites are separated by the distance l_p.

The model, defined by eqs 1−3, is considered in a wide pore

$$U_1(x) = \begin{cases} \infty, & x \le 0 \\ \infty, & x \ge l_x \\ 0, & l_x > x > 0 \end{cases} \tag{4}$$

A sketch of the simulation box is shown in Figure 2. To

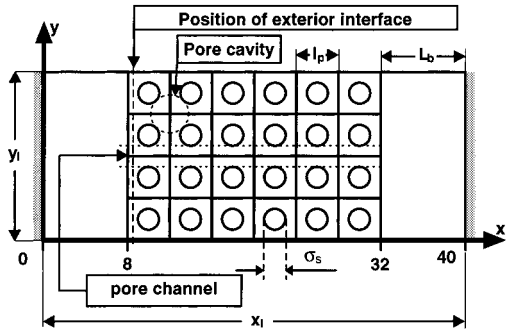

Figure 2. The geometry of the simulation cell and the definition of the coordinate system.

investigate this model, we have performed NVT Monte Carlo simulations, similar to refs 27 and 28. The unit cell in the xy plane is a rectangular with length l_x in x direction and l_y in y direction. Similar to ref 21, the membrane consists of six layers of particles along x axis and is infinite along y axis. Periodic boundary conditions have been used in y direction. The distance between a pore wall and membrane exterior is denoted L_b, $L_b = 0.5(l_x - 6l_p)$, see Figure 2. The membrane particles are rigidly fixed in their positions. An initial configuration for the fluid particles is prepared by inserting the particles into the available space. We have verified that the results do not depend on the initial configuration by performing some additional runs, i.e., we have checked that the equilibrium state describing partitioning of the fluid in the membrane-free space and inside the membrane is unique, independent of the starting conditions.

The displacement scheme for fluid species consists of translational and orientational displacement. The parameters for both displacements have been chosen to provide a total acceptance ratio around 30%.

The systems were equilibrated for at least 10^5 simulational steps. A production run, during which the averages have been obtained, consists of at least 10^6 steps. Care was taken so that equilibration was reached. We have evaluated the symmetry of the density profiles with respect to the membrane center, the symmetry of the contact value for the DP of fluid particles on the walls of a wide pore, the stability of the bulk density from run to run, and the fluctuations of the energy per particle. For the fluid densities that were considered, we have taken care to obtain a sufficiently wide bulk region for the fluid. We have defined the bulk part of the cell in between the wall of a wide pore and a set of membrane particles as that in which the density profile is constant up to fluctuations. Always, for low and intermediate densities we have used the following box dimensions, $l_x = 40$, and $l_y = 16$, and we have obtained a bulk region whose width is of the order of 4-6 fluid particle diameters. However, in the case of the highest density studied $\rho = 0.599$, it was necessary to increase the size of the simulational box ($l_x = 46$, $l_y = 16$) and the number of particles to be sure of the stability of the properties of the bulk fluid.

3. Results and Discussion

In this work we restrict ourselves to the (10) symmetry of the outer surface of the crystalline membrane. The parameters of our simulations and some of the results are given in Table 1. Throughout this work we consider only one model for membrane particles: $\sigma_s = 2$ and $l_p = 4$; the membrane represents a slit that is infinite along the y axis and of width 20 (the width is defined between centers of exposed membrane particles) along the x axis, see Figure 2.

We start the discussion with the results obtained for nonassociating particles ($\beta\epsilon_{\text{as}} = 0$) and then proceed with the

TABLE 1: The MC Simulation Results for Nonassociative Disks (N_f is the number of discs in the simulation cell)

N_f	ρ_b	ρ_m	α	β_p
56	0.1148	0.084	0.732	0.138
85	0.1722	0.131	0.761	0.230
141	0.2771	0.221	0.798	0.449
226	0.4285	0.362	0.846	0.999
271	0.5093	0.439	0.868	1.447
336	0.6198	0.555	0.895	2.361
393[a]	0.6169	0.551	0.896	2.337

[a] In 393 run the box with the length $l_x = 46$ has been used.

description of the partitioning of a dimerizing fluid. For the nonassociating system, we have performed six simulations which cover a range of nominal or average densities (the number of discs in the cell divided by its area) from 0.1 to 0.59; this latter case has been studied in ref 21. The number of particles has been changed in a box with given length, see Table 1, to obtain different densities. The density profiles, $\rho(x, y)$ have been calculated, as usual, from the number of particles in a square, the grid in x and y is equal to $\Delta = 0.05$. The bulk fluid density, ρ_b is the value obtained in the region where the profile between a hard wall and the surface of the membrane remains constant, except for the fluctuations. This bulk value appeared slightly larger than the nominal density for all the cases studied. Throughout this work, we present unnormalized density profiles, these can be transformed to the corresponding one-particle distribution functions simply by dividing the profiles by their value in the bulk region of the box.

A set of projections of the density profiles is presented in Figures 3 and 4. The lateral variation of the density profile, i.e., in the y plane at fixed x, is shown in Figure 3. The graph in part a of this figure corresponds to the x plane in which the fluid particles touch the membrane spheres of the outer plane, $x = 8.5$. This is the plane in which the lateral (along y axis) density profile varies most strongly. We call this plane the sliding parallel plane. Maxima of the fluid density are observed in front of membrane particles (due to adsorption), whereas in front of the pore channels the density is minimal. If one moves slightly farther from the membrane into the bulk $x = 8.0$, the range of variation of density decreases (Figure 3b). We call this plane the outer parallel plane. In the case of a high bulk density, $\rho_b = 0.509$, the fluid packing effects yield a maxima in front of the membrane channels, in contrast to the case of the contact plane ($x = 8.5$). For a low density bulk fluid, $\rho_b = 0.277$, these trends are not observed. It is of interest to mention that in the center of the first pore channel along y (and in subsequent channels), i.e., at $x = 12$, the lateral variation of density is very similar to that in the $x = 8.0$ plane; only the amplitude of variation of the density is larger in the interior of the membrane than outside (Figure 3c).

In Figure 4 the density profiles along the normal to the membrane surface are analyzed. In part a of this figure, the profile along the center of the pore channel ($y = 0$) is shown. Observe that the density profile at a higher fluid density, $\rho_b = 0.509$, exhibits periodicity; variation in the magnitude of maxima and minima is seen only in the regions of x that correspond to the exposed layers of membrane particles. It is of interest to note that the density is higher in the crossing points of the channels, whereas in the narrowest places of the pore, i.e., in the interstices between two particles, the density is lower. At a low density, $\rho_b = 0.277$, the density distribution in the center of the pore channel differs from the previous case. Due to the preferential adsorption of the fluid particles on the larger membrane particles it appears that the density in the interstices is higher than in the pore crossing. Obviously, these trends

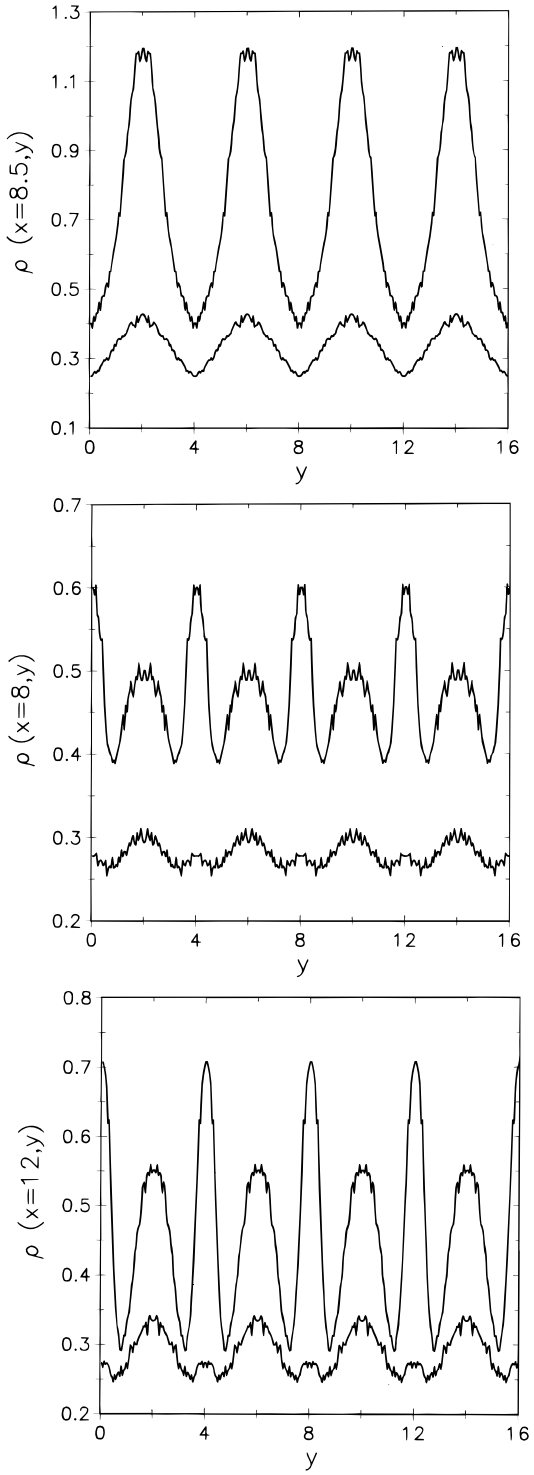

Figure 3. The lateral variation of the density profile for nonassociating discs along y axis: in the sliding parallel plane with respect to the membrane spheres (a), in the outer parallel plane, $x = 8.0$ (b), and inside the membrane in the center of the first inner pore channel, $x = 12$ (c). In all cases, the upper curves are for higher density $\rho = 0.509$; the lower curves correspond to a lower density $\rho = 0.277$.

result from packing fraction effects. In the sliding plane ($y = 0.5$) along x axis, we observe almost perfect periodicity for both densities; only in the case of the lower density, is the magnitude of the oscillations smaller, Figure 4b. At the higher density there is a small bump at the entrance of the membrane pore in this plane. This reflects the adsorption of discs at the entrance. A similar bump is observed on the cut along the line passing through the centers of membrane particles, $y = 2$. This reflects the weak layering of the bulk fluid close to a membrane particle

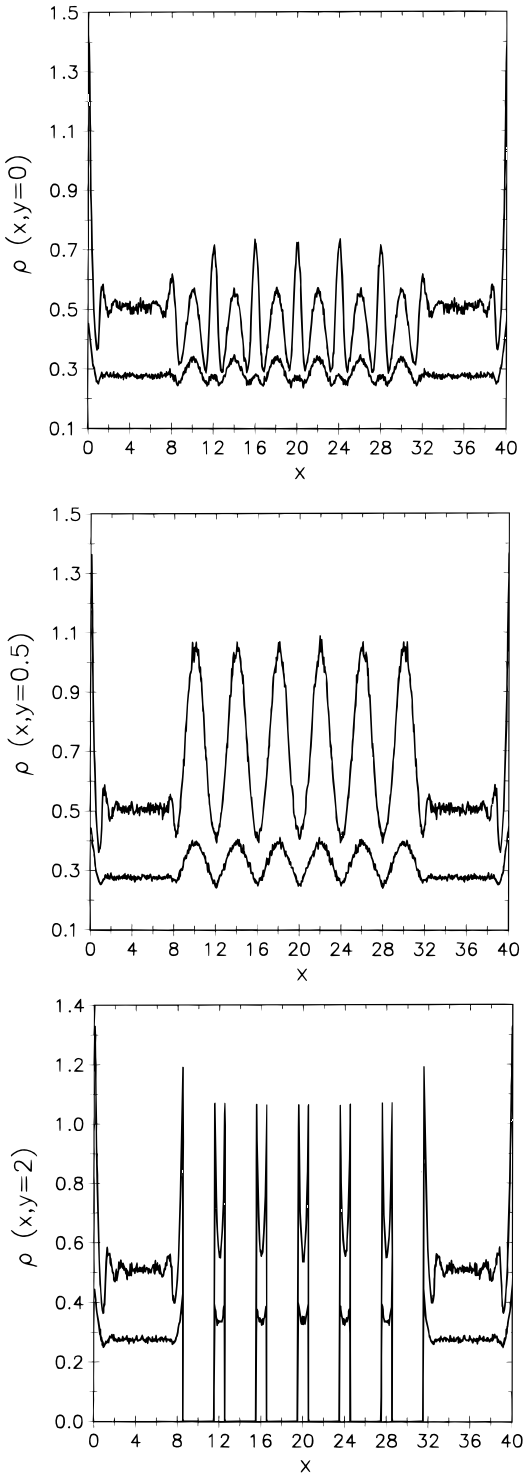

Figure 4. The normal variation of the density profile for nonassociating discs: in the center of a pore channel ($y = 0$) (a); in the sliding plane along x axis, $y = 0.5$ (b); and along the line through the centers of membrane particles of the layer in x direction, $y = 2$ (c). In all cases, the upper curves are for higher density $\rho = 0.509$; the lower curves correspond to a lower density $\rho = 0.509$.

that is qualitatively similar to the case of a hard wall, Figure 4c. A tendency for the adsorption of the fluid particles on the membrane species is observed along this cut of the density profile. Actually, the density is perturbed only in the exterior of the membrane. In its interior the shape of the profile is periodic following the positions of the membrane particles.

It is useful to discuss one technical issue briefly. In the case of the highest density $\rho_b = 0.599$, our simulations have shown that the "bulk region" does not extend appreciably. Therefore,

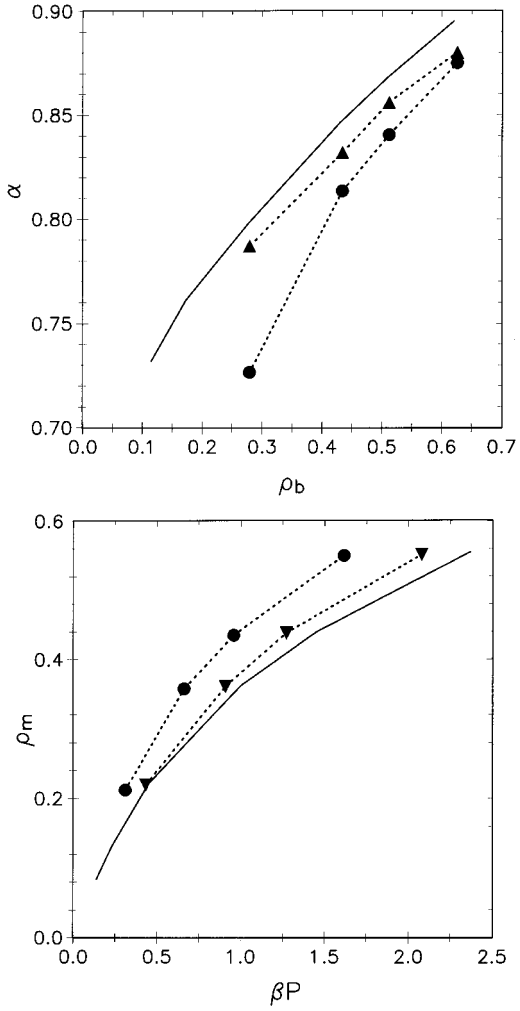

Figure 5. The dependence of the overall partition coefficients on the bulk density (a) and the adsorption isotherms (b) for a fluid of associating discs at $\beta\epsilon_{as} = 0$ (solid line), $\beta\epsilon_{as} = 5$ (triangles), and $\beta\epsilon_{as} = 10$ (circles).

one would expect that the presence of a hard wall of a wide pore may influence the density distribution close to the membrane surface. By comparing the averaged density profile[21] in simulations with a smaller and a larger box with a larger number of particles ($l_x = 46$) where the latter simulation yields a larger bulk region, we have verified that the results obtained for $\rho_b = 0.599$ are not altered.

From the contact value of the density profile on a hard wall, i.e., at $x = 0$, we obtain the value for the pressure βP according to the contact theorem: $\beta P = \rho_b$ ($x = 0$). In evaluating the contact value, we have interpolated the values of the density close to the wide pore wall. To evaluate the fluid partitioning, we have calculated the density of the particles in the interior of the membrane, i.e. in the region where the density profiles on x keep similar shape. Only close to the outer layer of the membrane are the density profiles perturbed with respect to the membrane interior. The values for the fluid density in the interior, ρ_m, were obtained in the region $14 < x < 20$, similarly to ref 21, i.e., we have calculated the number of particles in that region and normalized it by the area free of matrix particles. Then the partition coefficient α is obtained from $\alpha = \rho_m/\rho_b$.

It was found that the partition coefficient for a nonassociative fluid of discs increases with increasing bulk fluid density, see Figure 5a. Possibly, saturation can be obtained in the region of even higher bulk densities than we study (note that close packing for a one-component fluid of discs is observed at $\rho_b = 1.15$). The adsorption isotherm is shown in Figure 5b. Our

TABLE 2: The MC Simulation Results for Associative Disks

	$\beta\epsilon_{as}$						$\beta\epsilon_{as} = 10$					
N_f	ρ_b	ρ_m	α	β_p	X_0^m	X_0^b	ρ_b	ρ_m	α	β_p	X_0^m	X_0^b
141	0.279	0.2196	0.787	0.433	0.890	0.857	0.291	0.212	0.727	0.311	0.219	0.187
226	0.434	0.3610	0.832	0.908	0.797	0.763	0.440	0.358	0.814	0.661	0.156	0.141
271	0.512	0.4380	0.856	1.271	0.734	0.703	0.520	0.435	0.841	0.957	0.122	0.114
336	0.626	0.5510	0.880	2.079	0.650	0.617	0.627	0.5487	0.875	1.615	0.096	0.099

[a] The parameter α is the overall partition coefficient for particles irrespecively to their participation in bonds. The fractions of monomers X_0^m, X_0^b are for the membrane interior and the bulk fluid, respectively.

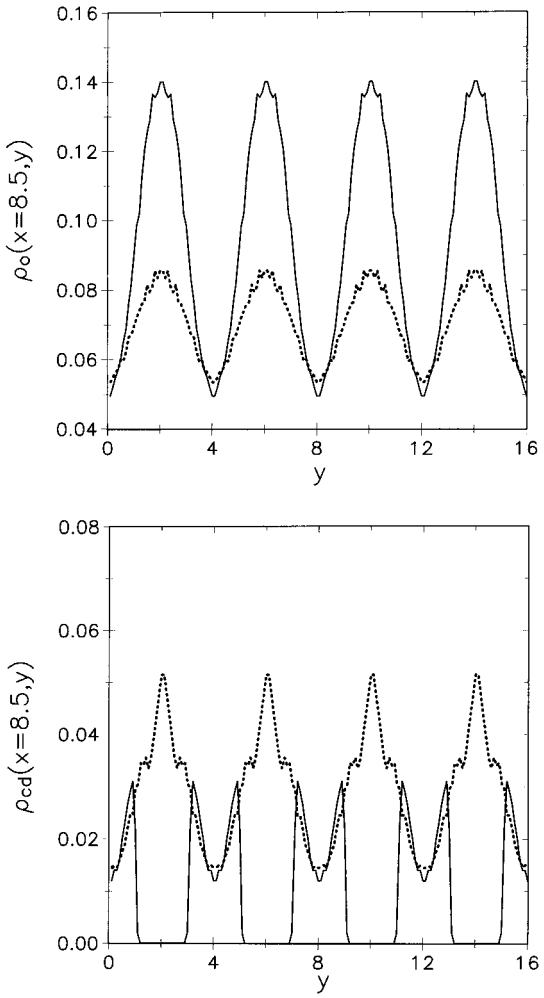

Figure 6. The lateral variation at $x = 8.5$ of the density profile for monomers (a) and the distribution of center of mass of dimers (b) along y axis for associating disc fluid at, $\beta\epsilon_{as} = 10$. In a, the solid line is for high density fluid, $\rho = 0.52$, whereas the dashed line is for a low density, $\rho = 0.29$. In b, the solid and dashed line correspond to the distribution of dimers with normal and parallel orientation with respect to the membrane exposed plane for the case of a high density fluid, $\rho = 0.52$.

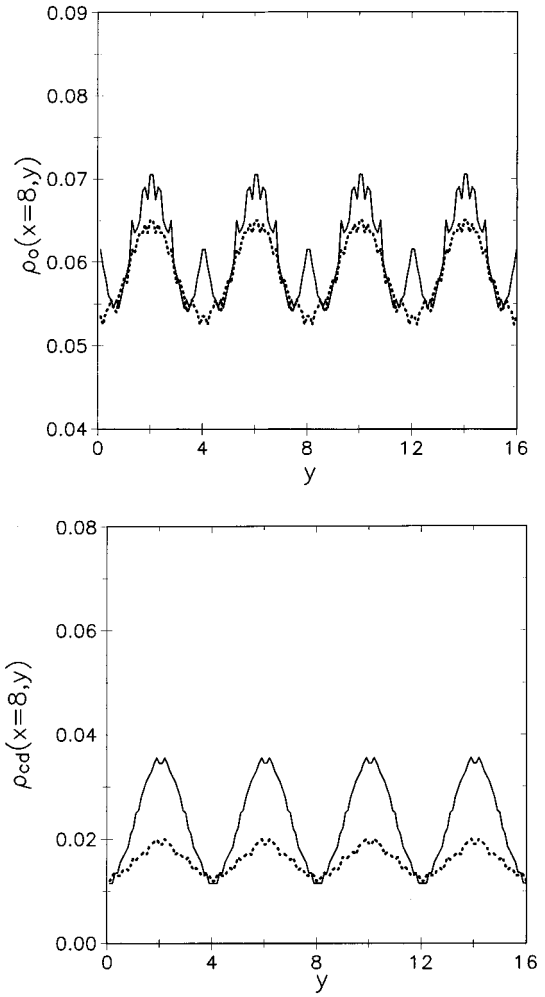

Figure 7. The same as in Figure 5 but in the plane $x = 8$. The nomenclature of lines in both fragments is similar to that in the fragments of Figure 5.

result for the highest fluid pressure coincides with that given in ref 21 for similar conditions. Adsorption increases with increasing pressure. For higher pressures, there is a tendency for saturation. The results for associating discs are also given in Figure 5a,b, but we will discuss them after inspecting the density profiles.

In Table 2 we present the results obtained for the total density of fluid particles in the bulk region and in the membrane interior, both these regions are defined similarly to the nonassociative case. In the case of an associative fluid, we define the total density $\rho(x, y)$ as a sum of densities of unbonded monomers, $\rho_0(x, y)$ and of those monomers that belong to dimers, $\rho_1(x, y)$; $\rho(x, y) = \rho_0(x, y) + \rho_1(x, y)$. The values for the densities and for pressures are given in Table 2, at $\beta\epsilon_{as} = 5$ and $\beta\epsilon_{as} = 10$. We observe that the pressure increases with increasing density at fixed association energy and decreases with increasing association energy at given density, as expected. The values for the overall partition coefficient, irrespective of the bonding states of the fluid particles, are given in Figure 5a. We observe that the values for α are appreciably lower at $\beta\epsilon_{as} = 10$ than at $\beta\epsilon_{as} = 0$. This serves as a manifestation of the lower partitioning due to an increasing fraction of dimer species in a fluid with increasing association energy. However, it appears more sensible to obtain a comparison of partitioning for free monomers and dimers separately, because the composition of our fluid at a given parameter of association energy changes with density. The overall partition coefficient does not yield insight into the equilibria between the bulk and membrane of monomers and dimers. We will discuss these data below. However, it is evident that, at a fixed fluid pressure, the overall

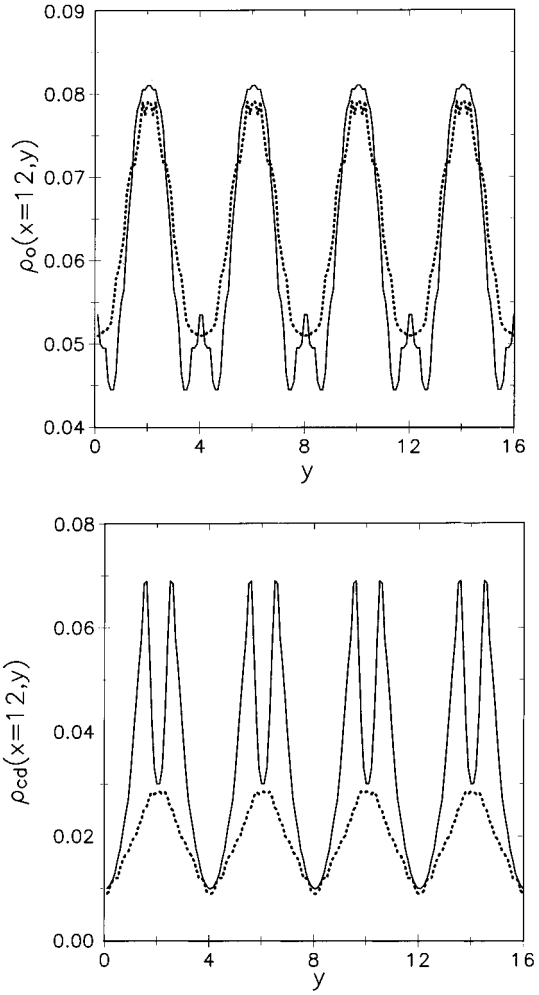

Figure 8. The same as in Figure 5 but in the plane $x = 12$. The nomenclature of lines in both fragments is similar to that in the fragments of Figure 5.

density in the membrane is higher for a higher $\beta\epsilon_{as}$, because of adsorption of dimers. In other words, a higher density dimerizing fluid in the membrane is needed to produce similar pressure for a nonassociating fluid outside of the membrane body.

To obtain clear evidence on the density distributions and partitioning of associating fluid through the membrane, we present the density profiles for the case of a high association energy, $\beta\epsilon_{as} = 10$ (Figures 6−8). We consider first the density profiles of the free monomers and the center of mass of the dimers, $\rho_{cd}(x, y)$ along the sliding parallel plane, $x = 8.5$, Figure 6, and in the outer plane, $x = 8.0$ (Figure 7). Monomers prefer to be adsorbed on the exposed membrane particles at a high density, $\rho_b = 0.52$ and at a low density $\rho_b = 0.29$ (Figure 6a). At the high density state, the bulk fluid is highly dimerized; the bulk fraction of dimers, $\chi_d^b = 0.443$ ($\chi_d^b = \rho_d^b/\rho_b$). The density of dimers close to the membrane particles is much lower than for the monomers. Still, the dimers adsorbed on the outer membrane particles prefer a parallel orientation with respect to the membrane, Figure 6b, similarly to the orientation of dimers on a hard wall. In front of the pore channels, the density of the dimers that are both parallel and normal to the membrane is negligible. In a slightly exposed plane, $x = 8$, the variation of the monomer and dimer density is lower (Figure 7), compared to the sliding plane, $x = 8.5$. Dimers with a normal orientation prefer to be situated in front of the membrane particles.

In the center of the first pore channel along y ($x = 12$) the density of the monomers is inhomogeneous with maxima in

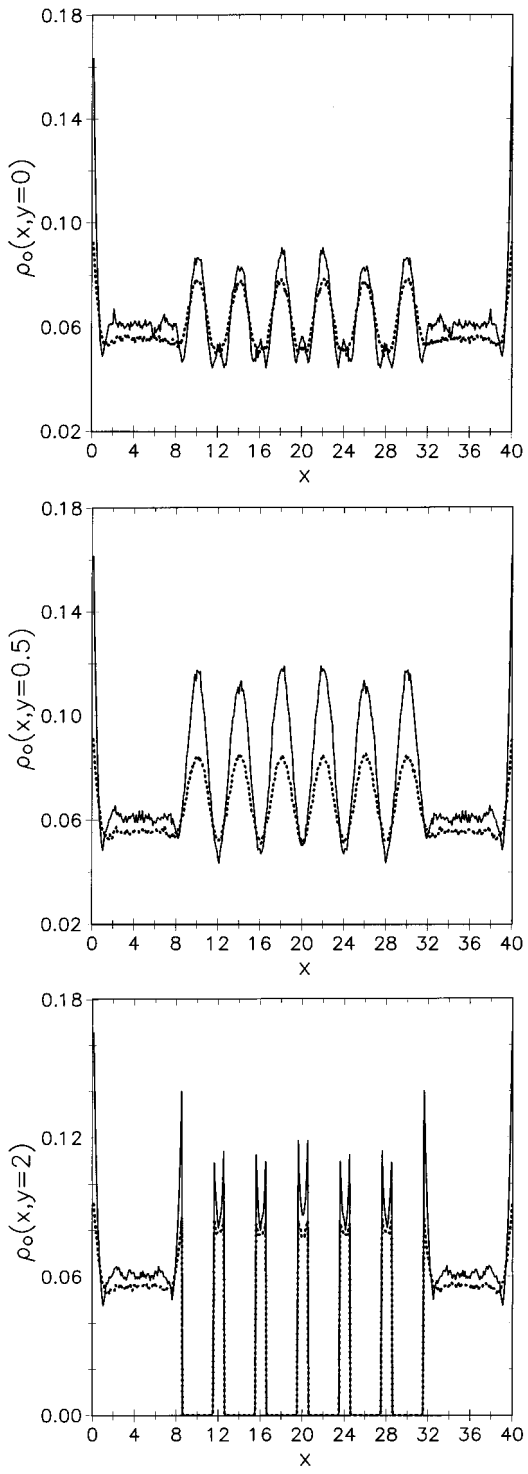

Figure 9. The normal variation of the density profile of monomers along x axis: in the center of a pore channel ($y = 0$) (a); in the sliding plane along x axis, $y = 0.5$ (b); and along the line through the centers of membrane particles of the layer in x direction, $y = 2$ (c). In all cases, the solid lines are for higher density $\rho = 0.522$, while the dashed lines correspond to a lower density $\rho = 0.29$. The value for the association energy is $\beta\epsilon_{as} = 10$.

the interstices of the membrane particles (Figure 8a). We also observe a higher probability density of finding dimers in a pore channel that are oriented normally (with respect to the membrane outer plane); one of the monomers belonging to a dimer is adsorbed on a membrane particle (Figure 8b).

In Figure 9 we show the density of monomers along x axis in the center of a pore channel ($y = 0$), in a normal sliding plane ($y = 0.5$) and at $y = 2$ for $\rho_b = 0.52$. It is important to

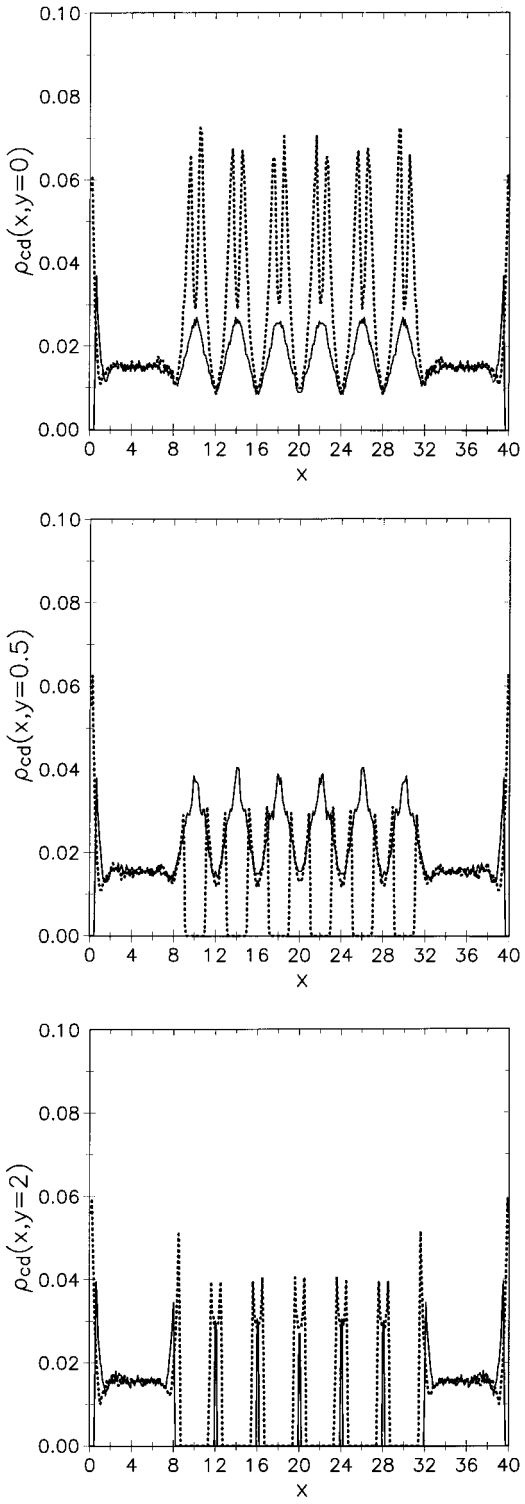

Figure 10. The profiles of the dimer center of mass density distribution for dimers with parallel (dashed lines) and normal (solid lines) orientation with respect to the outer membrane plane at an association energy $\beta\epsilon_{as} = 10$. In a, b, and c, the coordinate y is 0, 0.5, and 2.0, respectively. The fluid density is $\rho = 0.52$.

note the effect of adsorption of the fluid particles on the membrane obstacles, which results in a low monomer density in the pore crossings, i.e., in membrane cavities. Similar distributions for dimers are shown in Figure 10. It appears that dimers parallel to the membrane surface (normal to the channel) can be found with highest probability in the interstices between the matrix particles. Their density is even slightly higher than on a hard wall at $\rho_b = 0.52$ (Figure 10a). In the normal sliding plane ($y = 0.5$) the dimers are parallel to the pore channels,

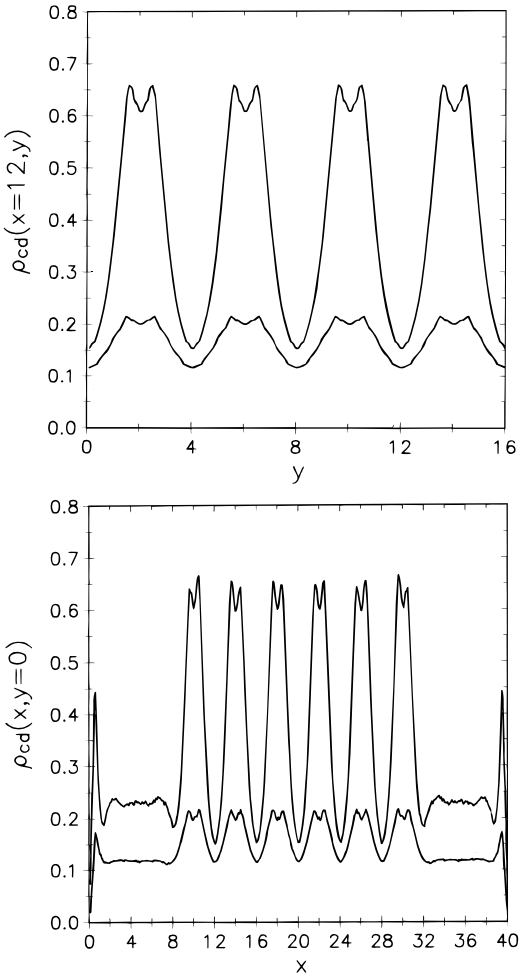

Figure 11. The profiles of the dimer center of mass density distribution for dimers with an arbitrary orientation in the center of a membrane channel along y and x axis in a and b, respectively. The fluid is at $\beta\epsilon_{as} = 10$; the upper curves are for $\rho = 0.52$, whereas the lower curves are for $\rho = 0.29$.

however, their density is low. The density profile of dimers at $\rho_b = 0.52$ in the membrane channels along x and y, irrespective of their orientation, is shown in Figure 11. We conclude that dimer density is much larger in the pore interstices than in the matrix cavities.

Finally in Figure 12, we present the partition coefficients for monomers and bonded particles belonging to dimers in the chemically associating disc fluid at $\beta\epsilon_{as} = 5$ and $\beta\epsilon_{as} = 10$. Higher energy leads to higher dimerization of the bulk fluid. We observe that the partition coefficient of the monomers increases with increasing bulk density; it saturates and then decreases in the region of high densities. The partition coefficient of the bonded species is higher for high bulk fluid densities, i.e., at high pressures, than for low densities. Comparing the partition coefficients of the unbonded and bonded species, we see that the monomer fraction is higher than that of the bonded particles in the membrane, as expected. Only at a high association energy, $\beta\epsilon_{as} = 10$, and a high density is a crossover observed, such that partition coefficient of bonded species becomes higher than that for monomers. This behavior can be explained as follows. For high association energy the fraction of dimerized species in the bulk nonlinearly depends on fluid density. In the region of high densities the degree of dimerization of the bulk fluid saturates. However, the adsorbed fluid is characterized by a lower density. The fraction of dimers in the adsorbed fluid increases with increasing density (pressure), whereas in the bulk fluid it increases less, in the region of high

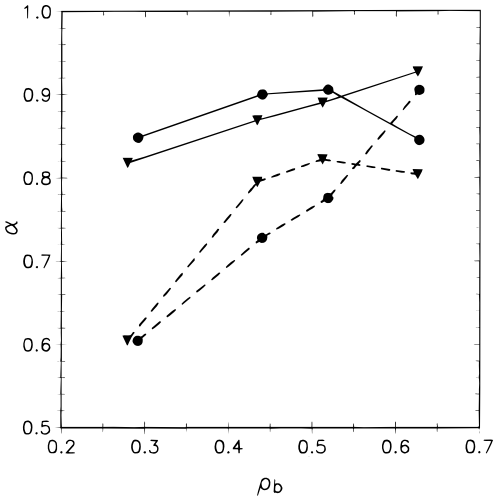

Figure 12. The dependence of the partition coefficients on the bulk fluid density for monomers (solid lines) and for particles belonging to dimers, i.e., for bonded particles (dashed lines). The association energy is $\beta\epsilon_{as} = 5$ (triangles) and $\beta\epsilon_{as} = 10$ (circles).

densities and for high association energy. These trends express a shape selectivity of the membrane with respect of the size of particles at different densities of a dimerizing fluid.

4. Conclusions

In this work we have investigated the equilibrium between a dimerizing fluid of hard discs in the bulk and in a crystalline membrane using Monte Carlo computer simulations. In the absence of association, the partition coefficient of fluid species increases with increasing pressure, as expected. In the case of the partitioning of a dimerizing fluid, we have found that monomers penetrate into the membrane body more easier than dimers, This is a reflection of the shape selectivity of the membrane. The partition coefficient of monomers is higher than for dimers in a wide region of densities. Only for a highly dimerized bulk fluid at high density have we observed the possibility that the partition coefficient of the dimers is slightly higher than for the monomers. We have investigated the normal and lateral distributions of monomers and dimers through the crystalline membrane body. We have seen that the normal variation of the profiles inside the membrane is periodic; only close to the membrane surfaces does the distribution of particles differ slightly from the distribution in the bulk interior. However, the normal and lateral variation of the density profiles is largest close to the exterior of the membrane surfaces. It appears that the density of particles, both monomers and dimers is higher in the interstices between membrane particles, whereas in the membrane pore cavities, i.e., in the crossings of pores, the density is lower. This is a clear manifestation of the adsorption effects of fluid particles on the surface of the larger membrane particles.

This model suggests several interesting extensions which are worth studying. Partitioning of chain fluids, formed as a result of the chemical association, would be of interest. On the other hand, more sophisticated models for the interactions between the fluid particles as well as of their interaction with the membrane species would permit an investigation of phase transitions in a model chemically associating fluid adsorbed in a regular porous network. The inclusion of the effects of chemical association between adsorbed fluid particles and membrane obstacles will make the model closer to the problem of fluid adsorption in simple models of zeolite structures. We hope to investigate some of these problems with a more sophisticated simulational methods in forthcoming publications.

Acknowledgment. This work was supported in parts by NSF under Grant CHE96-01971, by the American Chemical Society, Grant ACS-PRF 31573-AC9, by Silicon Graphics, Inc.—Cray Research of Mexico under its University Research and Development Grant Program, and by DGAPA of the UNAM under Research Project IN20779. Y.D. is grateful to the PEEI program of the UNAM for its financial support of his postdoctoral stay at IQ of the UNAM.

References and Notes

(1) Pizio, O.; Henderson, D.; Sokołowski, S. *J. Phys. Chem.* **1995**, *99*, 2408.
(2) Pizio, O.; Henderson, D.; Sokołowski, S. *Mol. Phys.* **1995**, *85*, 407.
(3) Henderson, D.; Sokołowski, S.; Pizio, O. *J. Chem. Phys.* **1995**, *102*, 9048.
(4) Pizio, O.; Henderson, D.; Sokołowski, S. *J. Colloid. Interface Sci.* **1995**, *173*, 254.
(5) Kalyuzhnyi, Yu. V.; Pizio, O.; Sokołowski, S. *Chem. Phys. Lett.* **1995**, *242*, 297.
(6) Pizio, O.; Sokołowski, S. *Phys. Rev. E* **1996**, *53*, 820.
(7) Trokhymchuk, A.; Pizio, O.; Sokołowski, S. *J. Coll. Interface Sci.* **1996**, *178*, 436.
(8) Holovko, M. F.; Vakarin, E. V. *Mol. Phys.* **1994**, *85*, 1057.
(9) Holovko, M. F.; Vakarin, E. V.; Duda, Yu. *Chem. Phys. Lett.* **1995**, *233*, 420.
(10) Segura, C. J.; Chapman, W. G. *Mol. Phys.* **1995**, *86*, 415.
(11) Segura, C. J.; Chapman, W. G.; Shukla, K. P. *Mol. Phys.* **1997**, *90*, 759.
(12) Muller, E. A.; Vega, L. F.; Gubbins, K. E.; Rull, L. F. *Mol. Phys.* **1995**, *85*, 9.
(13) Vega, L. F., Muller, E. A.; Rull, L. F.; Gubbins, K. E. *Mol. Simul.* **1995**, *15*, 141.
(14) Miyahara, M.; Gubbins, K. E. *J. Chem. Phys.* **1997**, *106*, 2865.
(15) Henderson, D., Kovalenko, A.; Pizio, O.; Sokołowski, S. *Physica A* **1996**, *231*, 254.
(16) Kovalenko, A.; Pizio, O.; Henderson, D.; Sokołowski, S. *J. Coll. Interface Sci.* **1996**, *182*, 407.
(17) Trokhymchuk, A., Pizio, O.; Henderson, D.; Sokołowski, S. *J. Phys. Chem.* **1996**, *100*, 5941.
(18) Trokhymchuk, A.; Pizio, O.; Holovko, M.; Sokołowski, S. *J. Phys. Chem.* **1996**, *100*, 17004.
(19) Trokhymchuk, A.; Pizio, O.; Henderson, D.; Sokołowski, S. *J. Chem. Phys.* **1997**, *106*, 220.
(20) Pizio, O.; Trokhymchuk, A.; Henderson, D.; Labík, S. *J. Colloid. Interface Sci.* **1997**, *191*, 86.
(21) Dong, W.; Bigot, B. *Phys. Rev. E* **1994**, *49*, 2184.
(22) Yethiraj, A.; Hall, C. K. *Mol. Phys.* **1991**, *73*, 503.
(23) Theodorou, D.; Wei, I. *J. Catal.* **1983**, *83*, 205.
(24) Vermesse, J.; Levesque, D. *Mol. Phys.* **1992**, *77*, 837.
(25) Vermesse, J.; Levesque, D. *J. Chem. Phys.* **1995**, *101*, 9063.
(26) Wertheim, M. S. *J. Chem. Phys.* **1986**, *85*, 2929.
(27) Ghonasgi, D.; Chapman, W. G. *Mol. Phys.* **1993**, *79*, 291.
(28) Chapman, W. G.; Jackson, G.; Gubbins, K. E. *Mol. Phys.* **1988**, *65*, 1057.